Optical and Quantum Electronics (2021) 53:248
https://doi.org/10.1007/s11082-021-02884-1

Si-based photodiode and material characterization of TiO_2 thin film

Hüseyin Kaan Kaplan[1] · Ali Olkun[1] · Sertan Kemal Akay[1] · Suat Pat[2]

Received: 31 October 2020 / Accepted: 12 April 2021
© The Author(s), under exclusive licence to Springer Science+Business Media, LLC, part of Springer Nature 2021

Abstract
This study proposes a different technique known as the thermionic vacuum arc to produce a TiO_2/Si heterojunction photodiode with better electrical properties than literature like the ideality factor indicating that the method is very suitable to form an outstanding quality heterojunction interface. The heterojunction is highly sensitive to different light intensities and has stable photocurrent characteristics as a photodiode. Structural and morphological properties of the produced TiO_2/Si heterostructure surfaces were investigated via XRD and AFM, respectively. According to XRD analysis, it was observed that the TiO_2 thin film was in a polycrystalline structure with the Anatase and Brookite phases. Also, the film surface is homogenous, and a low roughness value was measured as 3 nm. The thin film thickness and the bandgap values (E_g) were determined based on optical methods. The electrical parameters of TiO_2 thin film, such as conductivity type, charge carrier density, and mobility, were also determined by Hall Effect Measurement. The Ag/TiO2/Si/Ag heterojunction device characteristics were determined by conducting the current-voltage (I-V) measurement. The ideality factor (n) and the barrier height (Φ_b) values were determined as 1.7 and 0.65 eV, respectively. The photo-response performance was measured via transient photocurrent (I-T) measurements for different light intensities.

Keywords TiO_2 · Heterojunction diode · Photodiode · Thermionic vacuum arc · Thin film

1 Introduction

Metal oxide materials have many essential roles in health science, biology, chemistry, material science, and physics due to their chemical and electronic properties (Bharti 2020). As a metal oxide material of Titanium dioxide (TiO_2) is a non-toxic, chemically stable semiconductor material with a wide-bandgap. TiO_2 can be found under atmospheric pressure in three crystal forms: Rutile, Anatase, and Brookite (Bharti 2020; Aarik et al. 1995; Şilik et al. 2017). In the literature, TiO_2 thin films have been produced by many different

✉ Hüseyin Kaan Kaplan
kaplanhkaan@gmail.com

[1] Department of Physics, Faculty of Arts and Sciences, Bursa Uludağ University, 16059 Görükle, Bursa, Turkey

[2] Physics Department, Eskisehir Osmangazi University, 26480 Eskisehir, Turkey

Published online: 27 April 2021

methods such as sol–gel (Pacheco et al. 1998; Alam and Cameron 2002; Sonawane and Dongare 2006; Hanini et al. 2019; Erdal et al. 2019), sol–gel spin coating (Vorotilov et al. 1992; Wang et al. 2002; Manole et al. 2013; Malliga et al. 2014); hydrothermal synthesis (Cao et al. 2011; Ji et al. 2017), chemical bath deposition (Taşdemir et al. 2016), e-beam evaporation (Chakrabartty et al. 2014), plasma-enhanced chemical vapor deposition (PECVD) (Lee et al. 1994), atomic layer deposition (ALD) (Aarik et al. 1995; Aydin et al. 2014), RF magnetron sputtering (Tanemura et al. 2003; Xie et al. 2015), DC reactive sputtering (Ju et al. 2013), thermal oxidation (Hossein-Babaei et al. 2012; Lajvardi and Jahangiri 2016), thermionic vacuum arc (TVA) (Şilik et al. 2017; Şenay et al. 2017)), and pulsed laser deposition (PLD) (Rao et al. 2016).

TiO_2 has various uses to prevent UV rays from the sun due to the high UV absorption rate. TiO_2 has a potential for self-cleaning and sterilization applications due to the photocatalytic properties. It provides the decomposition of organic residues and materials such as fungal bacteria thanks to the sunlight or UV light, which is illuminated to the surface of the thin film (Sonawane and Dongare 2006). Also, applications of TiO_2 thin films includes many areas such as chemical gas sensors (Xie et al. 2015), photocatalytic device applications (Sonawane and Dongare 2006), electrochromic applications (Şilik et al. 2017), electronic and optoelectronic applications as heterojunction diodes (Erdal et al. 2019), solar cells, and photodetectors (Bharti 2020; Aarik et al. 1995; Alam and Cameron 2002; Cao et al. 2011; Hossein-Babaei et al. 2012; Lajvardi and Jahangiri 2016; Şenay et al. 2017). Optoelectronic devices produced in the form of thin films in recent years are of great interest. Notably, photodiodes have an important place due to their applications in electronics and electronic communication. In the literature, Si/TiO_2 based and TiO_2/Metal based photodiodes were produced with different techniques. Ji et al. reported that they had produced TiO2/Si heterojunction-based UV–Visible-light photodiodes with hydrothermal synthesis (Ji et al. 2017). Chakrabartty et al. announced an Au/TiO_2(NP)/SiO_x/Si TiO2 NPs based UV-A Schottky photodiode (Chakrabartty et al. 2014). Hossein-Babaei et al. reported a TiO_2/Ag Schottky UV photodiode (Hossein-Babaei et al. 2012). Lajvardi and Jahangiri announced a Ni/TiO_2 UV Schottky photodiode (Lajvardi and Jahangiri 2016).

In this study, the thermionic vacuum arc (TVA) method was used to deposit TiO_2 thin films. The TVA technique generates plasma of the material that is going to be deposited and does not require any precursor or carrier gas. Also, TVA is a rapid technique for producing pure and homogeneous thin films, and the system is inexpensive to operate (Şilik et al. 2017; Şenay et al. 2017). TiO_2 thin films were grown onto glass and n-Si substrates to form a TiO_2/Si heterojunction device and material analysis. An Ag/TiO_2/Si/Ag p-n heterojunction was produced from TiO_2 thin film deposited on the n-type silicon substrate. The optical, electronic, structural, and surface properties of TiO_2 thin film coated on glass and silicon were investigated. The device parameters of Ag/TiO_2/Si/Ag heterojunction photodiode were also studied in detail.

2 Experimental details

In this study, (100) oriented, $1-10\ \Omega$ cm, 500 µm thick, one side polished, n-type Si wafers, and microscope slides were used as deposition substrates. Alfa Aesar's 99.9% purity anatase Titanium (IV) Oxide (TiO_2) and Lesker's W dimple boat source were used as deposition material and anode material pot, respectively. The TiO_2 thin films, deposited on n-Si and glass substrates by using a physical vapor deposition method named

Thermionic Vacuum Arc (TVA) that creating plasma discharge of deposition material. Before deposition of TiO_2 thin film, Si and glass substrates were both cleaned ultrasonically with DI water, acetone, and isopropyl alcohol for 10 min for each step. Si substrate, also chemically-etched in 10% HF acid solution for 1 min to remove the native oxide layer. Subsequently, an Ag film thermally evaporated on the non-polished side of Si wafer with a thickness of 100 nm and rapidly annealed in 5 N-pure Ar flow at 350 °C for 5 min to make ohmic-back-contact. Afterward, the cleaned substrates were placed on substrate-holder in the TVA chamber, and the system evacuated to a base pressure of 9.0×10^{-5} Torr. After that, the cathode filament current slowly increased to the value of 16.5 A with an applied voltage up to 12 V until it glows incandescent. Then, the anode acceleration voltage was gradually increased to 450 V (with 0.15 A discharge current), where glowing plasma discharge occurred. These deposition conditions were maintained for 6 min with the deposition pressure of 1.1×10^{-4} Torr and continued for another 6 min under 9.0×10^{-5} Torr after 5 min break. Samples were left under vacuum after deposition for 60 min to establish the thermal equilibrium. Using a shadow mask, 1.5 mm diameter dot-shaped 100 nm thick Ag contacts were thermally evaporated on TiO_2 thin film, which deposited on n-Si substrates to form the Ag/TiO_2/Si/Ag heterojunction device.

The surface morphology and topography of the TiO_2/Si samples were examined by using Ambios Q-scope Atomic Force Microscope (AFM), and Carl Zeiss Gemini 300 model Field Emission Gun Scanning Electron Microscope (FESEM) surface images were recorded. TiO_2 thin film thickness and refractive index versus wavelength data were measured with FilMetrics F20 Thin Film Measurement System, and the film thickness was measured as 120 nm. Optical absorption, transmittance, and reflectance spectra of TiO_2 thin film were measured using Shimadzu UV-2600 UV–Vis spectrophotometer to evaluate the optical properties. TiO_2 thin film's electrical parameters such as conductivity type, charge carrier density, mobility, conductivity, and resistivity were measured at room temperature using the Ecopia HMS 3000 Hall Effect Measurement system. The Ag/TiO_2/Si/Ag heterojunction device's electrical and optoelectrical properties were determined by measurements performed at room temperature using FYTRONIX FY 7000 Sourcemeter combined with FYTRONIX FY 7000 Solar Simulator.

3 Findings and discussion

3.1 Structural and morphological features

The X-ray diffraction measurement of the TiO_2/Si sample at room temperature was conducted with Bruker AXS Discover D8 diffractometer, and the XRD pattern is depicted in Fig. 1. The diffraction angles (2θ) of the TiO_2 were determined as 32.958°, 61.687°, and 65.875°, which belongs to the Brookite and Anatase phases. The crystal phases and the corresponding miller indices were determined with the International Centre for Diffraction Data (ICDD) PDF-2 database. According to ICDD PDF no: 01-075-1582 and 00-029-1360, the two small peaks at 32.95° (020) and 65.875° (161) belong to the Brookite plane, respectively. The dominant peak at 61.687° (213) belongs to the Anatase phase, according to ICDD PDF no: 01–071-1169.

The crystallite sizes of the determined crystal phases were calculated using measured XRD data and the Scherer's equation given as (Cullity 1978):

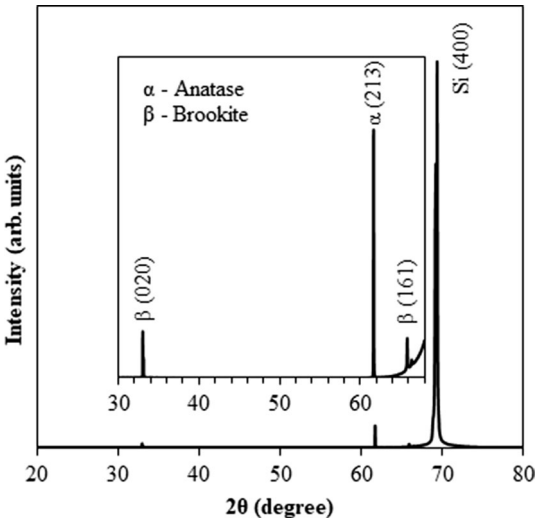


Fig. 1 XRD pattern of the TiO_2/Si sample

$$D(\text{nm}) = \frac{\text{K} \cdot \lambda}{\beta \cdot \cos\theta} \tag{1}$$

where K is a constant and equal to 0.9, λ is the X-ray wavelength of Cu-Kα, β is the FWHM value, and the θ is the diffraction angle value in radian. Although the crystallite sizes vary in the range of 110–200 nm, the crystallite size of the (213) oriented Anatase phase corresponding to 61.687° was determined to be approximately 200 nm. There are two other structural parameters called dislocation density (δ) and the microstrain (ε), which are expressed with Eqs. (2) and (3), respectively (Demirkol et al. 2019).

$$\delta = \frac{1}{D^2} \tag{2}$$

$$\varepsilon = \frac{\beta \cdot \cos\theta}{4} \tag{3}$$

Dislocation density and lattice strain values were calculated using XRD data, and all the results were listed in Table 1. These findings are quite different from a previous study on TiO_2 thin film deposited with TVA on ITO and FTO substrates (Şilik et al. 2017). Although this difference is due to the substrate difference, also affected by the differences in the deposition conditions like deposition pressure, duration, and thickness.

Table 1 XRD peaks and crystal parameters of the TiO_2/Si sample

2θ °	Crystal phase	Miller indices	Crystallite size (nm)	Dislocation density, $\delta \times 10^{-5}$ (lines/nm^{-2})	Micro-strain, $\varepsilon \times 10^{-5}$	ICDD PDF no
32.954	Brookite	(020)	111	8.039	1.096	01-075-1582
61.687	Anatase	(213)	200	2.499	0.338	01-071-1169
65.875	Brookite	(161)	119	7.041	0.535	00-029-1360

Ambios Q-scope Atomic Force Microscopy at room temperature in non-contact mode was used to examine TiO_2 thin film's morphological properties. AFM image of TiO_2 thin film in 3D is shown in Fig. 2a. In the measurements, the maximum distance between the peak and the valley was 27 nm. The average height was measured to be 16 nm, which can be seen from the inset histogram graph in Fig. 2a. Some important surface parameters, including root-mean-square (RMS) roughness, skewness (Ssk), and kurtosis (Skr) values, were obtained in morphological measurements. RMS roughness is defined as the square root of the surface height distribution and is used to calculate skewness and kurtosis values. RMS roughness value obtained by AFM measurement was found as 3 nm. Skewness (Ssk) value can be defined as the symmetry of the line on the surface, sensitive to peaks

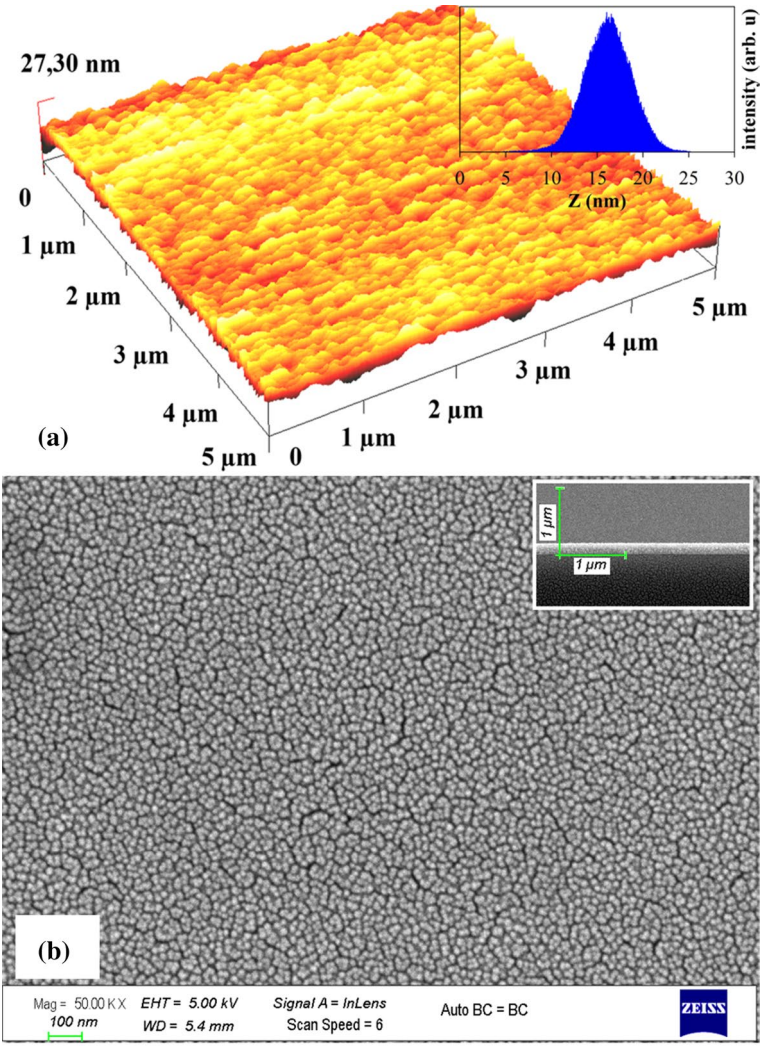


Fig. 2 **a** 3D AFM image with an inset figure of histogram, and **b** FESEM image with an inset figure of cross-section of the TiO_2/Si sample

and pits. The surface becomes more symmetrical as the skewness value approaches zero and more asymmetrical as it moves away from zero. A positive skew value means that the number of peaks is higher than the number of pits. If it is negative, it is understood that the pits are excessive. The skewness value (Ssk) was determined as − 0.201, which means pit numbers slightly higher than the number of peaks. The kurtosis (Skr) value is an expression that indicates that the surface is spiky or bumpy. When the kurtosis value is greater than 3, it means that the surface is spiky, and when it is less than 3, it means that the surface is bumpy. The kurtosis value in the study was obtained as 0.709, and this value shows us that the surface of the thin film is bumpy (Kumar and Rao 2012).

Carl Zeiss Gemini 300 model Field Emission Scanning Electron Microscope (FESEM) was used to examine the topographic and surface properties of the TiO_2 thin film. Figure 2b shows the surface image of TiO_2 thin film coated on silicon, and an inset figure shows the cross-section of the TiO_2/Si sample. The thickness was determined from the cross-section image as approximately 160 nm, corresponding to the sum of TiO_2 and Au–Pd films. It seems that the Au–Pd conductive coating is a bit thicker than the desired thickness, so it was changed the actual morphology of the TiO_2/Si surface. From the SEM image, it is seen that there are some cracks on the film surface, which is probably because of the original grain boundaries.

When AFM and SEM images are compared, it seems that they are compatible with each other by means of film homogeneity. Both images in Fig. 2a and b shows that the film surfaces highly uniform and smooth. It is seen from the AFM image that the grain diameters are varying approximately sub-hundred nanometers to a few hundred nanometers, which is also confirming the grains sizes calculated from XRD measurement. As seen from the cross-section image given as an inset image of Fig. 2b, the material's thickness coincides with the thickness determined via optical measurement. Approximately 40 nm of 160 nm total thickness belongs to the Au–Pd film, deposited before SEM imaging.

3.2 Optical properties

The wavelength-dependent refractive index spectra of TiO_2 thin film and the film thickness were measured by the FilMetrics F20 thin film measurement system. The thickness of the film was measured, on average, 120 nm. Refractive index—Wavelength change is given in Fig. 3. The refractive index at 550 nm wavelength corresponding to the middle of the visible region was measured as $n = 1.7$. This value is quite close to the values of 1.8107

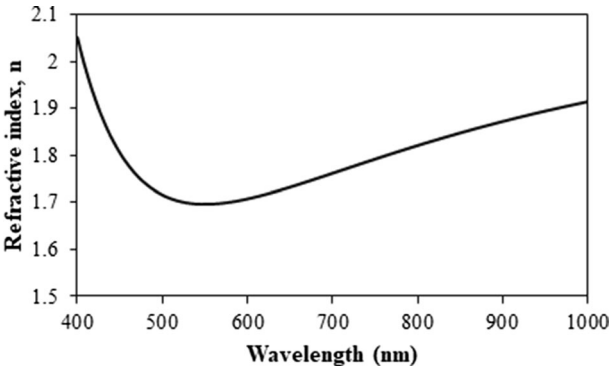


Fig. 3 Refractive index, n—Wavelength curve

obtained by Hanini et al. (2019), values of 1.827–1.858 by Pacheco et al. (1998), and values of 1.65–2.25 obtained by Vorotilov et al. (1992). Besides, it is small compared to the values of 2.04–1.94 obtained by Manole et al. (2013) and the 2.3 value obtained by Wang et al. (2002). The refractive index value obtained in this study is relatively low, and low refractive index materials can be used in optical and optoelectronic applications as anti-reflective coatings.

The optical absorption, transmittance, and reflectance spectra of TiO_2 thin film were measured in the 200–1100 nm wavelength range using Shimadzu UV-2600 Spectrophotometer. Plots of these measurements are given in Fig. 4.

The energy bandgap of a thin film can be calculated from the expression proposed by Tauc (1972) given with Eq. (4).

$$\alpha h\nu = C\left(h\nu - E_g\right)^m \tag{4}$$

Here, *α, h, ν, C, and m* represent the absorption coefficient, Planck's constant, photon frequency, a dimensionless constant, and an index that varies according to the transition state of the semiconductor's band structure, respectively. The value of m is determined as follows: $m = 1/2$ for allowed direct transitions, $m = 3/2$ for forbidden direct transitions, $m = 2$ for allowed indirect, and $m = 3$ for forbidden indirect transitions. It is expected to be equal to 0.5 for the Brookite phase since it is known as a direct bandgap semiconductor (Zhu and Gao 2014)**.** The Anatase phase should have a value of 2 because it is an indirect bandgap semiconductor (Zhu and Gao 2014). Since direct transitions are more likely to occur, it can be expected that the Brookite phase's direct transition would dominate the absorption characteristics of the TiO_2 thin film. According to Eq. (4) and the method proposed by

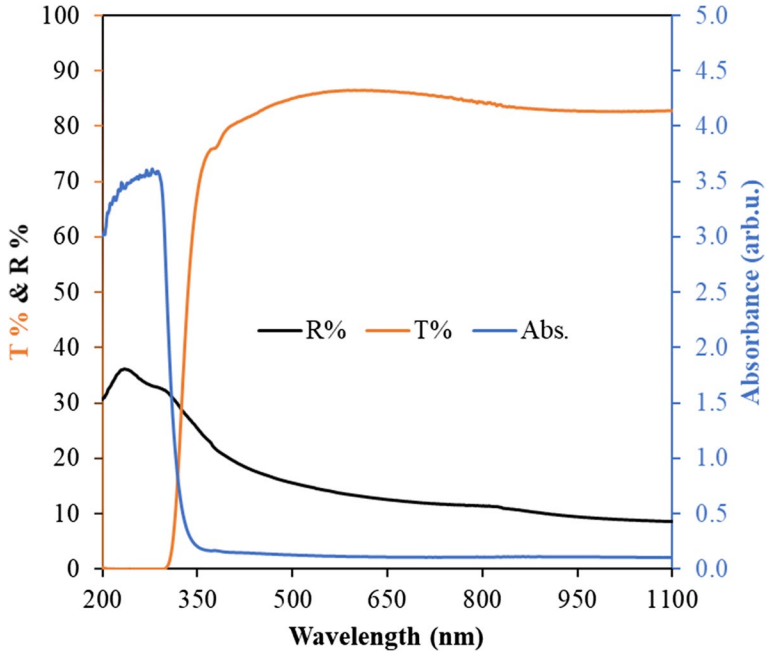


Fig. 4 The measured transmittance, reflectance, and absorption of the TiO_2 thin film sample as a function of optical wavelength

Bhattacharyya et al. (1992), the absorption coefficient can be given with Eq. (5) as a function of incident photon energy.

$$\alpha = \frac{C}{h\nu}\left(h\nu - E_g\right)^m \tag{5}$$

Then it can be rearranged as following equations named Eqs. (6) and (7):

$$\ln \alpha = \ln C - \ln h\nu + m \cdot \ln\left(h\nu - E_g\right) \tag{6}$$

$$\frac{d(\ln \alpha)}{d(h\nu)} = \frac{m}{h\nu - E_g} - \frac{1}{h\nu} \tag{7}$$

Equation (7) predicts that the "ln α versus hν" plot will have a divergence at the point where $h\nu = E_g$, enabling us to determine the energy bandgap value. In this study, the "ln α versus hν" plot didn't show a sufficiently clear divergence to determine the bandgap value. Therefore, the "d(ln α)/d(hν) versus hν" graph was used to determine the value of E_g similarly to Barreau et al. (2002). The bandgap value was obtained as $E_g = 3.84$ eV from the divergence point of the graph given with Fig. 5a. Using the obtained E_g value, ln (αhν) versus ln (hν – E_g) graph is plotted in Fig. 5b, and the "*m*" value is calculated as the slope of the linear graph. The value of *"m"* is found to be equal to the approximate value of 0.5, which is confirming the prediction that the allowed direct transition of the Brookite phase dominated the absorption characteristic of the TiO_2 thin-film.

A more accurate bandgap value than the one obtained above now can be calculated using the "m = 0.5" value and the Eq. (4) mentioned above. The curve "$(\alpha h\nu)^2$ – hν" obtained from the optical absorption spectrum data using Tauc expression is shown in Fig. 6. The bandgap value was obtained as $E_g = 3.85$ eV from the "$(\alpha h\nu)^2$ – hν" plot given with Fig. 6 by intercepting the "hν" axis for "$\alpha h\nu = 0$" using the linear section of the graph. Calculated E_g values with different studies are compared in Table 2. While the E_g value of TiO_2 thin film is compatible with some studies, it is calculated higher than the E_g value of some studies. This difference probably depends on the parameters that affect the structure of the produced film, such as production method, chamber pressure, deposition speed, deposition duration, and thickness (Şilik et al. 2017; Vorotilov et al. 1992; Wang et al. 2002; Malliga et al. 2014; Tanemura et al. 2003; Şenay et al. 2017).

The optical transmittance graph of the TiO_2 thin film is given in Fig. 4. As can be seen from the Figure, the highest transmittance value is 86.567%, which appears at 416 nm photon wavelength. It has also been found to have an average transmittance value of 85% in the visible region. These results are highly compatible with the literature (Şilik et al. 2017; Vorotilov et al. 1992; Wang et al. 2002; Malliga et al. 2014; Tanemura et al. 2003; Şenay et al. 2017; Bartic et al. 2013). Also, it is seen from Fig. 4, the TiO_2 thin film does not exhibit interference fringes. This behavior can be attributed to low refractive index value (n = 1.7), surface homogeneity, and low roughness value.

3.3 Electric properties

Hall Effect Measurement was performed at room temperature to determine the electrical properties of TiO_2 thin film. Values were defined as the average of ten consecutive measurements. The electrical conductivity type was determined to be p-type, so

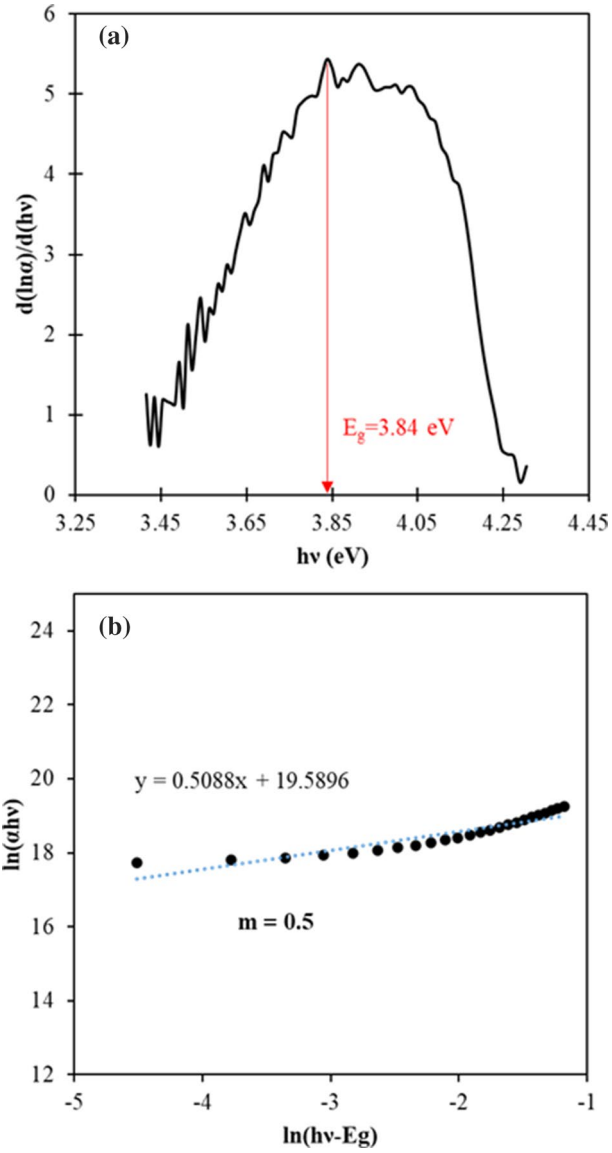


Fig. 5 **a** The graph of "d(ln α)/d(hν) versus hν" curve, **b** the plot of ln (αhν) versus ln (hν – E_g) for $E_g = 3.84$ eV

dominant charge carriers are holes with a density of 9.01×10^{12} cm^{-3}. The p-type conductivity in undoped TiO2 thin-films can be attributed possible titanium (Ti) vacancies or oxygen (O) interstitials in structure as Iancu et al. (2015) and Wang et al. (2015) explained in detailed. In addition to the charge carrier concentration, hole mobility, resistivity, conductivity, Magneto-Resistance, and Average Hall Coefficient values were determined as 9.01×10^{12} cm^{-3}, 19.91 cm^2/V s, $1.272 \times 10^{+5}$ Ω cm, 7.122×10^{-6} S/cm, $6.172 \times 10^{+9}$ Ω, and $2.863 \times 10^{+6}$ cm/C, respectively. Besides, these values are given in comparison with some literature data in Table 3.

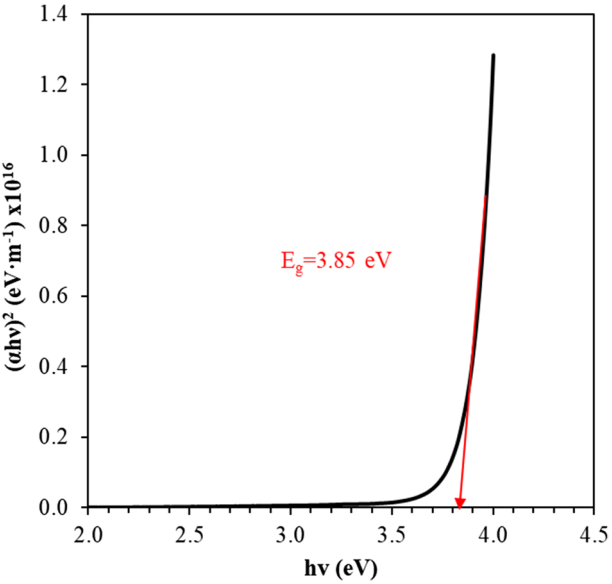


Fig. 6 Graph of $(\alpha h\nu)^2$ *versus* $h\nu$ showing the estimation of E_g value

Table 2 Comparison of bandgap energy of TiO_2 thin film with different studies

References	E_g (eV)	Coating method
This work	3.85	TVA
Şilik et al. (2017)	3.00	TVA
Malliga et al. (2014)	2.20–3.90	Sol–Gel Spin
Tanemura et al. (2003)	3.03–3.51	RF magnetron scattering
Şenay et al. (2017)	3.20	TVA
Sarıgül and Sorar (2016)	3.80–4.04	Sol–Gel Spin

3.4 Heterojunction diode properties

The room temperature current-voltage (I-V) measurements were performed to determine the diode characteristics of the produced Ag/TiO_2/Si/Ag heterojunction device in the dark and under 100 mW/cm^2 illumination, which corresponds to 1 sun (AM 1.5). The dark and under illumination I-V data plots were given in Fig. 7a, and the semi-logarithmic dark I-V graph was presented in Fig. 7b. Measurements were carried using the FYTRONIX FY 7000 Sourcemeter and FY 7000 Solar Simulators.

From the graph of dark I-V measurement data given in Fig. 7, it is seen that the heterojunction device has a diode (rectifier) characteristic. The rectification ratio at ± 3 V was calculated as approximately $I_F/I_R = 381$. According to the theory of thermionic emission (TE), which is also very useful to express the current transmission mechanism of heterojunction diodes, the current flowing through the diode can be written as Eq. (8) (Sze and Ng 1981):

Table 3 Electric properties of TiO_2 thin film and comparison with some studies in the literature

Refs	Conductivity type	Carrier density (cm^{-3})	Mobility ($cm^2/V{\cdot}s$)	Resistivity ($\Omega{\cdot}cm$)	Conductivity (S/cm)	Magneto-resistance (Ω)
This work	p	9.01×10^{12}	19.91	1.272×10^{5}	7.122×10^{-6}	$6.172\times10^{+9}$
Wang et al. 2002	–	–	–	0.26–10.1	3.85–0.01	–
Ji et al. 2017	n	1.4×10^{11}	–	2.0×10^{6}	–	–
Ji et al. 2017	n	6.9×10^{10}	–	2.6×10^{6}	–	–
Ji et al. 2017	n	3.1×10^{11}	–	1.3×10^{6}	–	–
Rao et al. 2016	–	–	–	4.46×10^{11}–1.98×10^{12}	–	–
Muaz et al. 2015	–	–	–	3.715×10^{12}	2.692×10^{-13}	–

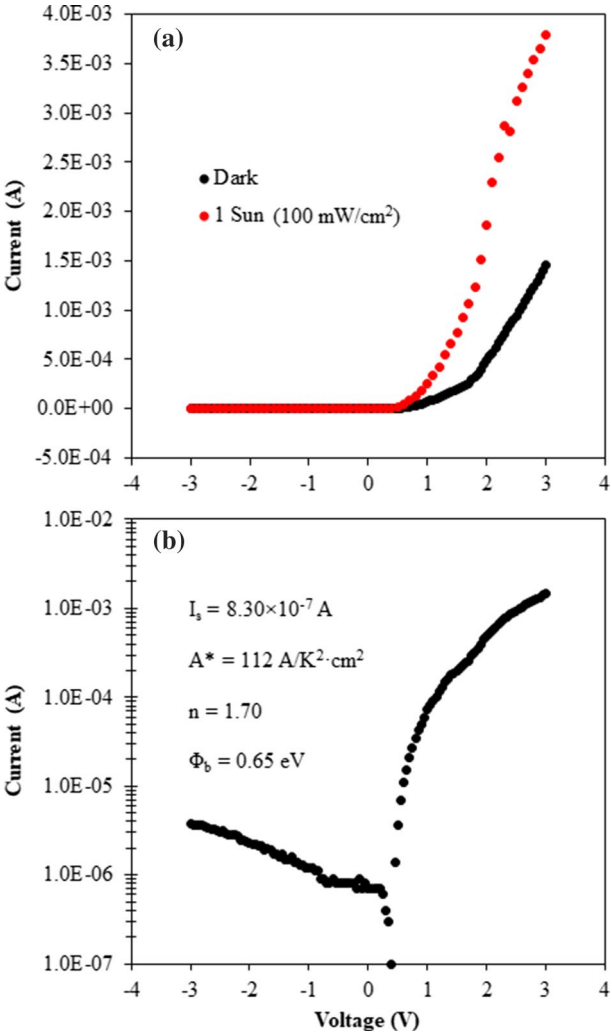


Fig. 7 Room temperature I-V graphs of Ag/*p*-TiO_2/*n*-Si/Ag heterojunction diode **a** dark and 1 Sun solar irradiation, and **b** semi-logarithmic dark I-V curve

$$I = I_S\left[\exp\left(\frac{qV}{nkT}\right) - 1\right] \tag{8}$$

Herein, I_S is the reverse saturation current, n is the ideality factor, q is the charge of the electron, V is the voltage applied to the heterojunction, k is the Boltzmann's constant, and T is the absolute temperature. The reverse saturation current (I_S) is expressed as follows (Eq. (9)).

$$I_S = A \cdot A^* \cdot T^2\left[\exp\left(\frac{q\Phi_b}{kT}\right) - 1\right] \tag{9}$$

where the Φ_b is the barrier height, A is the active diode area, and the A* is the Richardson constant. I_S value was determined by intercepting the current-axis by extrapolating the

part where the curve is linear in the semi-logarithmic I-V curve's negative bias region. The Richardson constant value is 112 A K^{-2} m^{-2} for *n*-type Si (Andrews and Lepselter 1970). Using Eq. (9) an expression for barrier height, Φ_b can be written as follows

$$\Phi_b = \frac{kT}{q} \cdot \ln\left(\frac{A \cdot A^* \cdot T^2}{I_S}\right) \tag{10}$$

By using Eq. (10) and the reverse saturation current value $I_S = 8.3 \times 10^{-7}$ A obtained from the graph in Fig. 7b, the barrier height was calculated as $\Phi_b = 0.65$ eV. This value is relatively smaller than 0.74, 0.81 eV (Taşdemir et al. 2016), 0.71, 0.93 eV (Erdal et al. 2019), 0.7 eV (Chakrabartty et al. 2014) and very close to 0.66 eV (Aydin et al. 2014), and it is compatible with the literature. Another essential parameter mentioned above is the ideality factor *n*, which is expressed below with the Eq. (11) (Rhoderick and Williams 1988).

$$n = \frac{q}{kT} \cdot \left(\frac{dV}{d(\ln(I))}\right) \tag{11}$$

Its value was calculated as n = 1.7 from Eq. (11) by using semi-log I-V data represented in Fig. 7b. This value is very close to the ideal value of 1, representing the current flowing across the junction, obeys the pure thermionic emission mechanism. The deviation from the ideal value indicates that the current transport mechanism is affected by space charge limited current (SCLC) or tunneling as well as thermionic emission (Güllü 2019). Even so, values between 1 and 2 indicate that the current transport mechanism is highly obeying the thermionic emission mechanism (Güllü 2019; Kaya 2020). Also, ideality factor value obtained in this study is quite smaller compared to 11.4 (Chakrabartty et al. 2014), 9.66, 7.31, 1.8 (Ji et al. 2017), 5.19, 1.93 (Erdal et al. 2019), 8.39, 2.29 (Taşdemir et al. 2016), and 2.96 (Aydin et al. 2014).

In addition, transient photocurrent (I-T) measurements were made to examine the Ag/TiO2/Si/Ag heterojunction diode's photo-response and photodiode performance. The transient photocurrent measurements were carried out under five different light intensities (20, 40, 60, 80, 100 mW/cm^2) using a solar simulator at a constant bias voltage of 3 V. As can be seen from Fig. 8, while the dark current is as low as 0.6 mA, it has been observed that it has a high response speed with a very stable photocurrent at different irradiance intensities. For all illumination intensities, the photocurrent was instantly changed when the light turn-on and turn-off. These properties suggest that the Ag/TiO_2/Si/Ag heterojunction diode has good photodiode potential with its stable and swift response time.

4 Conclusion

The TiO_2 thin film's crystal structure produced on Si substrates by the TVA method was analyzed by XRD analysis. Surface morphology was examined with AFM, and it was observed that it has a low surface roughness of 3 nm and a homogeneous structure. Thin-film thickness was measured as 120 nm. It was determined by optical measurements and calculations that the TiO_2 thin film has high transmittance of 85% in the optical region of the EM spectrum and that the bandgap energy is $E_g = 3.85$ eV, which is in accordance with the literature. Unlike many other studies, the thin film's electrical parameters were determined by Hall Effect measurement, and it was observed that it was p-type. In addition, it has been observed from the I-V measurements that the

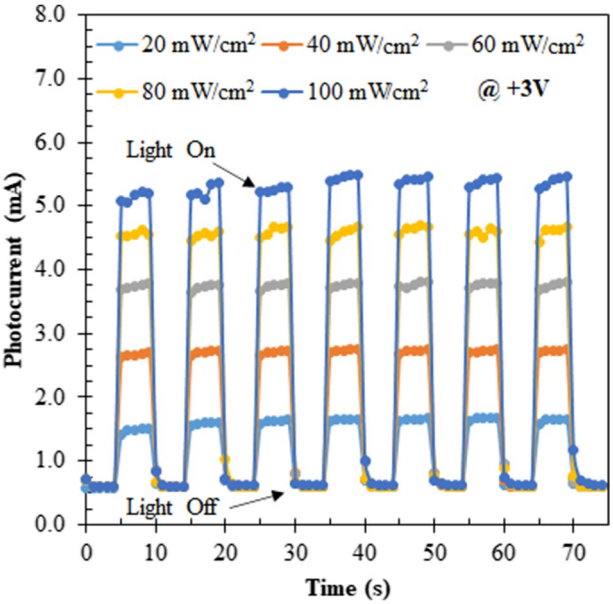


Fig. 8 Transient photocurrent graph at + 3 V bias voltage

produced Ag/TiO_2/Si/Ag heterojunction device shows diode characteristics with a good rectification ratio. The fundamental electrical parameters were calculated; the ideality factor value was found to be quite good compared to other studies in the literature, and the barrier height value (0.65 eV) was found in agreement with them. Moreover, the heterojunction diode was shown to have good light sensitivity, from I-V measurement under 1 sun (AM 1.5) irradiation and I-T measurements of different irradiance intensity.

These properties indicate that the Ag/TiO_2/Si/Ag heterojunction device has a fast and highly stable photodiode characteristic. According to these results, it can be said that the photodiode device is suitable for different applications for light detection or optical communication purposes in the UV–Visible range.

Acknowledgements We would like to thank TÜBİTAK for supporting Ph.D. students Hüseyin Kaan KAPLAN and Ali OLKUN with the BİDEB 2211/C Domestic Priority Areas Doctoral Scholarship Program and BİDEB 2244 Industrial Doctoral Scholarship Program.

Funding There is no financial support.

Code availability Not applicable.

Declarations

Conflict of interest The authors declare that they have no known competing financial interests or personal relationships that could have appeared to influence the work reported in this paper.

Availability of data and material The data that support the findings of this study are available on request from the corresponding author, [Kaplan, H.K.]. The data are not publicly available due to being part of ongoing study.

References

Aarik, J., Aidla, A., Uustare, T., Sammelselg, V.: Morphology and structure of TiO2 thin films grown by atomic layer deposition. J. Cryst. Growth **148**(3), 268–275 (1995). https://doi.org/10.1016/0022-0248(94)00874-4

Alam, M.J., Cameron, D.C.: Preparation and characterization of TiO_2 thin films by sol-gel method. J. Sol-Gel. Sci. Technol. **25**(2), 137–145 (2002). https://doi.org/10.1023/A:1019912312654

Andrews, J.M., Lepselter, M.P.: Reverse current-voltage characteristics of metal-silicide Schottky diodes. Solid-State Electron. **13**(7), 1011–1023 (1970)

Aydin, S.B., Yildiz, D.E., Çavuş, H.K., Şahingöz, R.: ALD TiO_2 thin film as dielectric for Al/p-Si Schottky diode. Bull. Mater. Sci. **37**(7), 1563–1568 (2014). https://doi.org/10.1007/s12034-014-0726-6

Barreau, N., Bernède, J.C., Marsillac, S.: Study of the new β-In2S3 containing Na thin films. Part II: optical and electrical characterization of thin films. J. Cryst. Growth **241**(1), 51–56 (2002). https://doi.org/10.1016/S0022-0248(02)01243-5

Bartic, M., Sacarescu, L., Harabagiu, V.: Optical and electrical properties of TiO_2 thin films deposited by sol-gel method. Rev. Roum. Chim. **58**(2–3), 105–111 (2013)

Bharti, B.: Surface modification of titanium dioxide TiO_2 thin films and their applications, (2020).

Bhattacharyya, D., Chaudhuri, S., Pal, A.K.: Bandgap and optical transitions in thin films from reflectance measurements. Vacuum **43**(4), 313–316 (1992). https://doi.org/10.1016/0042-207X(92)90163-Q

Cao, C., Hu, C., Wang, X., Wang, S., Tian, Y., Zhang, H.: UV sensor based on TiO_2 nanorod arrays on FTO thin film. Sens. Actuators B Chem. **156**(1), 114–119 (2011). https://doi.org/10.1016/j.snb.2011.03.080

Chakrabartty, S., Mondal, A., Sarkar, M.B., Choudhuri, B., Saha, A.K., Bhattacharyya, A.: TiO_2 nanoparticles arrays ultraviolet-A detector with Au Schottky contact. IEEE Photonics Technol. Lett. **26**(11), 1065–1068 (2014). https://doi.org/10.1109/LPT.2014.2313181

Cullity, B.D.: Elements of X-ray Diffraction, p. 149. Wesley Mass, Addison (1978)

Demirkol, U., Pat, S., Mohammadigharehbagh, R., Musaoğlu, C., Özgür, M., Elmas, S., Korkmaz, Ş: Determination of the structural, morphological and optical properties of graphene doped SnO thin films deposited by using thermionic vacuum arc technique. Phys. B **569**, 14–19 (2019). https://doi.org/10.1016/j.physb.2019.05.035

Erdal, M.O., Kocyigit, A., Yıldırım, M.: Temperature dependent current-voltage characteristics of Al/TiO_2/n-Si and Al/Cu: TiO_2/n-Si devices. Mater. Sci. Semicond. Process. **103**, 104620 (2019). https://doi.org/10.1016/j.mssp.2019.104620

Güllü, H.H.: Investigation of electrical properties of In/ZnIn2Te4/n-Si/Ag diode. Bull Mater Sci **42**, 89 (2019). https://doi.org/10.1007/s12034-019-1770-z

Hanini, F., Bouabellou, A., Bouachiba, Y., Taabouche, A., Kermiche, F., Mahtali, M., Daas, Z.: Elaboration and characterization of in doped TiO_2 thin films. Defect Diffus. Forum. **397**, 59–68 (2019)

Hossein-Babaei, F., Lajvardi, M.M., Boroumand, F.A.: Large area Ag–TiO2 UV radiation sensor fabricated on a thermally oxidized titanium chip. Sens. Actuators, A **173**(1), 116–121 (2012). https://doi.org/10.1016/j.sna.2011.10.028

Iancu, A.T., Logar, M., Park, J., Prinz, F.B.: Atomic layer deposition of undoped TiO_2 exhibiting p-type conductivity. ACS Appl. Mater. Interfaces. **7**(9), 5134–5140 (2015). https://doi.org/10.1021/am5072223

Ji, T., Liu, Q., Zou, R., Zhang, Y., Wang, L., Sang, L., Hu, J.: Enhanced UV-visible light photodetectors with a TiO_2/Si heterojunction using band engineering. J. Mater. Chem. C **5**(48), 12848–12856 (2017). https://doi.org/10.1039/c7tc04811d

Ju, Y., Wang, M., Wang, Y., Wang, S., Fu, C.: Electrical properties of amorphous titanium oxide thin films for bolometric application. Adv. Condens. Matter Phys. (2013). https://doi.org/10.1155/2013/365475

Kaya, S.: Nanostructure, optical and electrical properties of p-NiO/n-Si heterojunction diodes. Appl. Phys. A **126**, 636 (2020). https://doi.org/10.1007/s00339-020-03816-8

Kumar, B.R., Rao, T.S.: AFM studies on surface morphology, topography and texture of nanostructured zinc aluminum oxide thin films. Dig. J. Nanomater. Biostruct. **7**(4), 1881–1889 (2012)

Lajvardi, M. M., & Jahangiri, M. (2016). Ni/TiO_2 ultraviolet detector. In IOP Conf. Ser.: Mater. Sci. Eng. 108: 012031. https://doi.org/10.1088/1757-899X/108/1/012031

Lee, W.G., Woo, S.I., Kim, J.C., Choi, S.H., Oh, K.H.: Preparation and properties of amorphous TiO_2 thin films by plasma enhanced chemical vapor deposition. Thin Solid Films **237**(1–2), 105–111 (1994). https://doi.org/10.1016/0040-6090(94)90245-3

Malliga, P., Pandiarajan, J., Prithivikumaran, N., Neyvasagam, K.: Influence of film thickness on structural and optical properties of sol–gel spin coated TiO_2 thin film. IOSR J Appl Phys **6**(1), 22–28 (2014). https://doi.org/10.9790/4861-06112228

Manole, A.V., Dobromir, M., Girtan, M., Mallet, R., Rusu, G., Luca, D.: Optical properties of Nb-doped TiO_2 thin films prepared by sol–gel method. Ceram. Int. **39**(5), 4771–4776 (2013). https://doi.org/10.1016/j.ceramint.2012.11.066

Muaz, A.K.M., Hashim, U., Nadzirah, S., Al-Mufti, M.W., Ibrahim, F., Kwai Lin, T.: Electrical properties of nano-TiO_2 thin film prepared by sol-gel precipitation route using two-point probe method. Adv. Mater. Res. **1109**, 153–157 (2015)

Pacheco, F., Palomino, R., Martinez, G., Mendoza-Galvan, A., Talavera, R.R., Castano, V.M.: Optical characterization of titania thin films produced by the sol-gel method and doped with Co^{2+} at different concentrations. Appl. Opt. **37**(10), 1867–1872 (1998). https://doi.org/10.1364/AO.37.001867

Rao, M. C., Ravindranadh, K., & Shekhawat, M. S.: Structural and electrical properties of TiO_2 thin films. *AIP Conference Proceedings*, *1728*, 2–6. (2016). https://doi.org/10.1063/1.4946128

Rhoderick, E.H., Williams, R.H.: Metal-Semiconductor Contacts, 2nd edn. Oxford University Press, New York (1988)

Sarıgül, H., Sorar, İ: Optical and electrochromic properties of TiO_2 films prepared by Sol-Gel method. Marmara J Sci **28**(2), 81–88 (2016). https://doi.org/10.7240/mufbed.14319

Şenay, V., Özen, S., Pat, S., Geçici, B., Korkmaz, Ş: A new method for titania thin film production: thermionic vacuum arc method. J Thermoplast Composit Mater **30**(6), 808–815 (2017)

Şilik, E., Pat, S., Özen, S., Mohammadigharehbagh, R., Yudar, H.H., Musaoğlu, C., Korkmaz, Ş: Electrochromic properties of TiO_2 thin films grown by thermionic vacuum arc method. Thin Solid Films **640**, 27–32 (2017). https://doi.org/10.1016/j.tsf.2017.07.073

Sonawane, R.S., Dongare, M.K.: Sol–gel synthesis of Au/TiO_2 thin films for photocatalytic degradation of phenol in sunlight. J. Mol. Catal. A: Chem. **243**(1), 68–76 (2006). https://doi.org/10.1016/j.molcata.2005.07.043

Sze, S.M., Ng, K.K.: Physics of Semiconductor Devices, 3rd edn. John Wiley and Sons Inc., Hoboken, New Jersey (1981)

Tanemura, S., Miao, L., Jin, P., Kaneko, K., Terai, A., Nabatova-Gabain, N.: Optical properties of polycrystalline and epitaxial anatase and rutile TiO_2 thin films by RF magnetron sputtering. Appl. Surf. Sci. **212–213**, 654–660 (2003). https://doi.org/10.1016/s0169-4332(03)00015-1

Taşdemir, İH., Vural, Ö., Dökme, İ: Electrical characteristics of p-Si/TiO_2/Al and p-Si/TiO_2-Zr/Al Schottky devices. Phil. Mag. **96**(16), 1684–1693 (2016). https://doi.org/10.1080/14786435.2016.1178403

Tauc, J.C.: Optical Properties of Solid, p. 372. North-Holland, Amsterdam (1972)

Vorotilov, K.A., Orlova, E.V., Petrovsky, V.I.: Sol-gel TiO_2 films on silicon substrates. Thin Solid Films **207**(1–2), 180–184 (1992). https://doi.org/10.1016/0040-6090(92)90120-Z

Wang, Z., Helmersson, U., Käll, P.O.: Optical properties of anatase TiO_2 thin films prepared by aqueous sol–gel process at low temperature. Thin Solid Films **405**(1–2), 50–54 (2002). https://doi.org/10.1016/s0040-6090(01)01767-9

Wang, S., Pan, L., Song, J.J., Mi, W., Zou, J.J., Wang, L., Zhang, X.: Titanium-defected undoped anatase TiO_2 with p-type conductivity, room-temperature ferromagnetism, and remarkable photocatalytic performance. J. Am. Chem. Soc. **137**(8), 2975–2983 (2015). https://doi.org/10.1021/ja512047k

Xie, T., Sullivan, N., Steffens, K., Wen, B., Liu, G., Debnath, R., Motayed, A.: UV-assisted room-temperature chemiresistive NO_2 sensor based on TiO_2 thin film. J. Alloy. Compd. **653**, 255–259 (2015). https://doi.org/10.1016/j.jallcom.2015.09.021

Zhu, T., Gao, S.P.: The stability, electronic structure, and optical property of TiO_2 polymorphs. J. Phys. Chem. C **118**(21), 11385–11396 (2014). https://doi.org/10.1021/jp412462m

Publisher's Note Springer Nature remains neutral with regard to jurisdictional claims in published maps and institutional affiliations.